Cell

Article

A Memory System of Negative Polarity Cues Prevents Replicative Aging

Franz Meitinger,[1,5] Anton Khmelinskii,[2] Sandrine Morlot,[3] Bahtiyar Kurtulmus,[1] Saravanan Palani,[1,6] Amparo Andres-Pons,[1,7] Birgit Hub,[4] Michael Knop,[2] Gilles Charvin,[3] and Gislene Pereira[1,*]

[1]Molecular Biology of Centrosomes and Cilia, German Cancer Research Center (DKFZ), DKFZ-ZMBH Alliance, Im Neuenheimer Feld 581, Heidelberg 69120, Germany

[2]Center for Molecular Biology of the University of Heidelberg (ZMBH), DKFZ-ZMBH Alliance, 69120 Heidelberg, Germany

[3]Institut de Génétique et de Biologie Moléculaire et Cellulaire, 1 Rue Laurent Fries, 67400 Illkirch Cedex, France

[4]German Cancer Research Center (DKFZ), Im Neuenheimer Feld 280, 69120 Heidelberg, Germany

[5]Present address: Ludwig Institute for Cancer Research, 9500 Gilman Drive, CMM East, La Jolla, CA 92093, USA

[6]Present address: Division of Biomedical Cell Biology, Warwick Medical School, University of Warwick, Coventry CV4 7AL, UK

[7]Present address: European Molecular Biology Laboratory, Structural and Computational Biology Unit, Meyerhofstrasse 1, 69117 Heidelberg, Germany

*Correspondence: g.pereira@dkfz.de

http://dx.doi.org/10.1016/j.cell.2014.10.014

SUMMARY

Cdc42 is a highly conserved master regulator of cell polarity. Here, we investigated the mechanism by which yeast cells never re-establish polarity at cortical sites (cytokinesis remnants [CRMs]) that have previously supported Cdc42-mediated growth as a paradigm to mechanistically understand how Cdc42-inhibitory polarity cues are established. We revealed a two-step mechanism of loading the Cdc42 antagonist Nba1 into CRMs to mark these compartments as refractory for a second round of Cdc42 activation. Our data indicate that Nba1 together with a cortically tethered adaptor protein confers memory of previous polarization events to translate this spatial legacy into a biochemical signal that ensures the local singularity of Cdc42 activation. "Memory loss" mutants that repeatedly use the same polarity site over multiple generations display nuclear segregation defects and a shorter lifespan. Our work thus established CRMs as negative polarity cues that prevent Cdc42 reactivation to sustain the fitness of replicating cells.

INTRODUCTION

The establishment of cell polarity sites is fundamental for a plethora of cellular functions related to morphogenesis, differentiation, and/or proliferation of uni- and multicellular organisms (Bloch and Yalovsky, 2013; Dworkin, 2009; Heasman and Ridley, 2008; Howell and Lew, 2012; Iden and Collard, 2008; Li and Bowerman, 2010; Martin-Belmonte and Perez-Moreno, 2011; McCaffrey and Macara, 2009; Nelson, 2009; Noatynska et al., 2013). The Rho-GTPase Cdc42, initially described in yeast (Johnson and Pringle, 1990), is a master regulator of cell polarization and highly conserved among eukaryotes (Boureux et al., 2007; Etienne-Manneville, 2004). How Cdc42 polarity sites are regulated in space and time has been extensively studied over the past years (Casamayor and Snyder, 2002; Johnson et al., 2011; Park and Bi, 2007). However, much less is known about the molecular mechanisms involved in the establishment of polarity cue refractory to Cdc42 activation.

During G1 phase, yeast cells establish a polarity site from which the daughter cell will emerge. Polarity establishment depends on Rho GTPase Cdc42 (Park and Bi, 2007). The site of bud emergence (bud neck) will later be used in cytokinesis to separate the daughter from mother cell (Figure 1A) (Park and Bi, 2007; Wloka and Bi, 2012). The remnants of the cytokinetic machinery (bud scar or cytokinesis remnant [CRM]) are retained in the mother cell and can be visualized by transmission electron microscopy (TEM) or by specific dyes (Figure 1B) (Meitinger et al., 2013). CRMs mainly consist of extracellular matrix, which is encircled by a chitin-rich ring (Cabib et al., 1993). In addition, transmembrane proteins, including Rax1 and Rax2, protrude into the extra- and intracellular spaces (Kang et al., 2004). This indicates that CRMs may modulate intracellular processes. However, relatively little is known about the composition and function of CRMs. During the replicative lifetime, the aging mother cell accumulates increasing numbers of these CRMs over its cell surface (Casamayor and Snyder, 2002). Importantly, a new polarity site is never established within CRMs, indicating that Cdc42 activation cannot occur twice at the same site, even though the initiation event could be many generations after the cytokinesis that generated the remnant.

The molecular basis for the prevention of Cdc42 activation at CRMs remains to be established. Different GTPase-activating proteins (GAPs) contribute to the inhibition of Cdc42 at the cell-division site (Atkins et al., 2013; Tong et al., 2007). In addition, the scaffold protein Gps1 inhibits Cdc42 at the site of cytokinesis as part of a pathway working in parallel to the Cdc42 GAP Rga1 (Meitinger et al., 2013). However, neither Cdc42 GAPs nor Gps1 accumulate at old CRMs. Using a combination of proteomics, cell biology, and biochemical approaches, we identified a protein complex that is recruited to the cell-division site by Gps1 and inherited to CRMs in a Gps1 and Rax1-Rax2-dependent manner. We show that Nba1, a bud-neck-associated protein of unknown

function (Calvert et al., 2008), is the core component of this complex that is responsible for the prevention of Cdc42 activation in the remnant. Mutant cells that are unable to inhibit Cdc42 activation at CRMs display nuclear segregation defects and have markedly shorter lifespans. This study therefore identifies the molecular mechanism for a long-recognized phenomenon that keeps CRMs inactive for Cdc42-reactivation, thereby ensuring the longevity of asymmetrically dividing yeast cells.

RESULTS

Nap1, Nba1, and Nis1 Function with Gps1 in Cdc42 Inhibition

Nap1, Nba1, and Nis1 were previously identified as putative Gps1-interacting proteins (Meitinger et al., 2013). Nap1 is a conserved histone chaperone involved in chromatin assembly and morphogenesis (Ishimi and Kikuchi, 1991; Mortensen et al., 2002), whereas Nba1 and Nis1 are proteins of unknown function associated with the cell-division site (Calvert et al., 2008; Iwase and Toh-e, 2001). Using coimmunoprecipitation experiments, we established that Nap1, Nba1, and Nis1 interact with Gps1 (Figure 1C). Fluorescence microscopy analysis revealed that GFP-tagged Gps1, Nap1, Nba1, and Nis1 localize to the cell-division site (Figure 1D). This localization was cell-cycle-dependent for Nap1, Nba1, and Nis1 (Figures S1A and S1B available online). In contrast, only Nba1 and Nis1 localized to CRMs (Figure 1E).

Gps1 localized to the cell-division site independently of *NAP1*, *NBA1*, or *NIS1* (Figures 1F and S1C). Similarly, Nap1 localization to the cell-division site was not affected in *gps1*Δ, *nba1*Δ, or *nis1*Δ cells (Figures 1F and S1C). Nba1 failed to localize to the cell-division site in the absence of *GPS1* (Figures 1F and S1C), although its protein levels were unaffected by deletion of *GPS1* (Figure S1D). Nis1 localization to the cell-division site also required *GPS1*. Moreover, *NAP1* and *NBA1* were necessary for Nis1 localization to the cell-division site (Figures 1F and S1C). Consistent with this observation, coimmunoprecipitation of Nis1 with Gps1 was impaired in the absence of *NAP1* or *NBA1* (Figure 1C).

Interestingly, although GFP-tagged Gps1 and Nap1 did not localize to CRMs, both were necessary for Nba1 and Nis1 localization to CRMs (Figures 1G and S1C). Impaired localization of Nis1 to CRMs in *nap1*Δ cells was at least partially explained by reduced levels of Nis1-GFP in this mutant (Figure S1D). Furthermore, localization of Nba1 and Nis1 to CRMs was mutually dependent (Figure 1G). Together, we conclude that Gps1 and Nap1 are involved in recruiting Nba1 and Nis1 to the cell-division site, and in loading Nba1 and Nis1 to CRMs (Figures 1H).

Gps1 coordinates the activity of Cdc42 and Rho1, two members of the Rho family of small GTPases (Meitinger et al., 2013). In the absence of *GPS1,* abnormal activation of the Cdc42 GTPase causes rebudding inside the old cell-division site, resulting in the appearance of one or more concentric collars of cell wall material at the cell-division site in 30%–40% of the cells (Figure 1I) (Meitinger et al., 2013). In addition, deletion of *GPS1* also compromises the Rho1 cytokinetic pathway, leading to a thinning of the secondary septum (Meitinger et al., 2013). Transmission electron microscopy of *nap1*Δ, *nba1*Δ, and *nis1*Δ cells revealed multiple collars at the bud neck without any thinning of the secondary septum in all three mutants (Table 1A), suggesting that Nap1, Nba1, and Nis1 are involved in regulating Cdc42 but not Rho1. The multiple collar phenotype was more frequent in the *nba1Δ* strain (Table 1A), indicating that Nba1 plays a major role in Cdc42 inhibition. Together, these results established Nap1, Nba1, and Nis1 as Gps1-interacting proteins that are specifically involved in inhibiting the Cdc42 pathway. Furthermore, our findings suggest that inhibition of Cdc42 might not be restricted to the cell-division site but could also occur at CRMs, where Nba1 and Nis1 localize.

Nba1 Is Necessary and Sufficient to Inhibit Cdc42

We sought to understand how Gps1 interacts with Cdc42, Nap1, Nba1, and Nis1. Yeast two-hybrid experiments with Gps1 truncations suggested that Gps1 has specific binding domains for each of its interaction partners (Figures 2A and S2A). In vitro, recombinant Gps1$^{293–422}$ (a fragment of Gps1 containing the amino acid residues 293–422), Gps1$^{514–600}$ and Gps1$^{443–530}$ interacted directly and specifically with recombinant Nap1, Nba1, and Nis1, respectively (Figure 2B). Based on these results we generated a Gps1$^{\Delta513–598}$ mutant in which the Nba1 interaction domain was deleted. Nba1 failed to interact with Gps1$^{\Delta513–598}$ in yeast two hybrid (Figure 2C) and showed impaired localization to the cell-division site and CRMs in *gps1*$^{\Delta513–598}$ cells (Figures 2D and 2E). Notably, *gps1*$^{\Delta513–598}$ cells showed no defects in Rho1 regulation, as judged by the thickness of the secondary septum, yet exhibited multiple collar phenotype with frequency similar to that of *gps1Δ* and *nba1Δ* mutants (Table 1B). This observation suggests that Nba1 functions downstream of Gps1 in the Cdc42 inhibition pathway, and that the main role of Gps1 is to recruit Nba1 to the cell division site and CRMs.

If this model is correct, then artificial targeting of Nba1 to the cell-division site should eliminate the need for Gps1 in Cdc42 inhibition. We tested this possibility using the septin Shs1 tagged with the GFP-binding protein (GBP) (Rothbauer et al., 2008) to recruit GFP fusions to the cell-division site (Meitinger et al., 2013). Expression of *SHS1-GBP* in *NBA1-GFP gps1*Δ cells resulted in permanent association of Nba1-GFP with the cell-division site, partially restored the localization of Nba1-GFP to CRMs and partially rescued the growth defect of the *gps1Δ* mutant (Figures 2F–2H). Notably, artificial tethering of Nba1 to Shs1 rescued the multiple collar phenotype but not the secondary septum defect of *gps1Δ* cells (Table 1C), indicating that *NBA1-GFP gps1*Δ *SHS1-GBP* cells bypassed the requirement of Gps1 in the regulation of Cdc42 but not of Rho1. Similar results were obtained with *NIS1-GFP gps1Δ SHS1-GBP* cells (Figures S2B–S2D; Table 1D). However, Shs1-tethered Nis1 required *NBA1* for function, whereas Shs1-tethered Nba1 suppressed the *gps1*Δ growth defect even in the absence of *NIS1* (Figures 2H and S2D). Collectively, our data indicate that Gps1 recruits Nba1 and Nis1 to the cell-division site and CRMs, where Nba1 is necessary and sufficient to inhibit Cdc42 activation.

Nba1 Inhibits Binding of the GEF Cdc24 to GTP-Bound Rsr1

Next, we concentrated on the mechanism of Cdc42 inhibition by Nba1. Two parallel mechanisms contribute to the site-directed

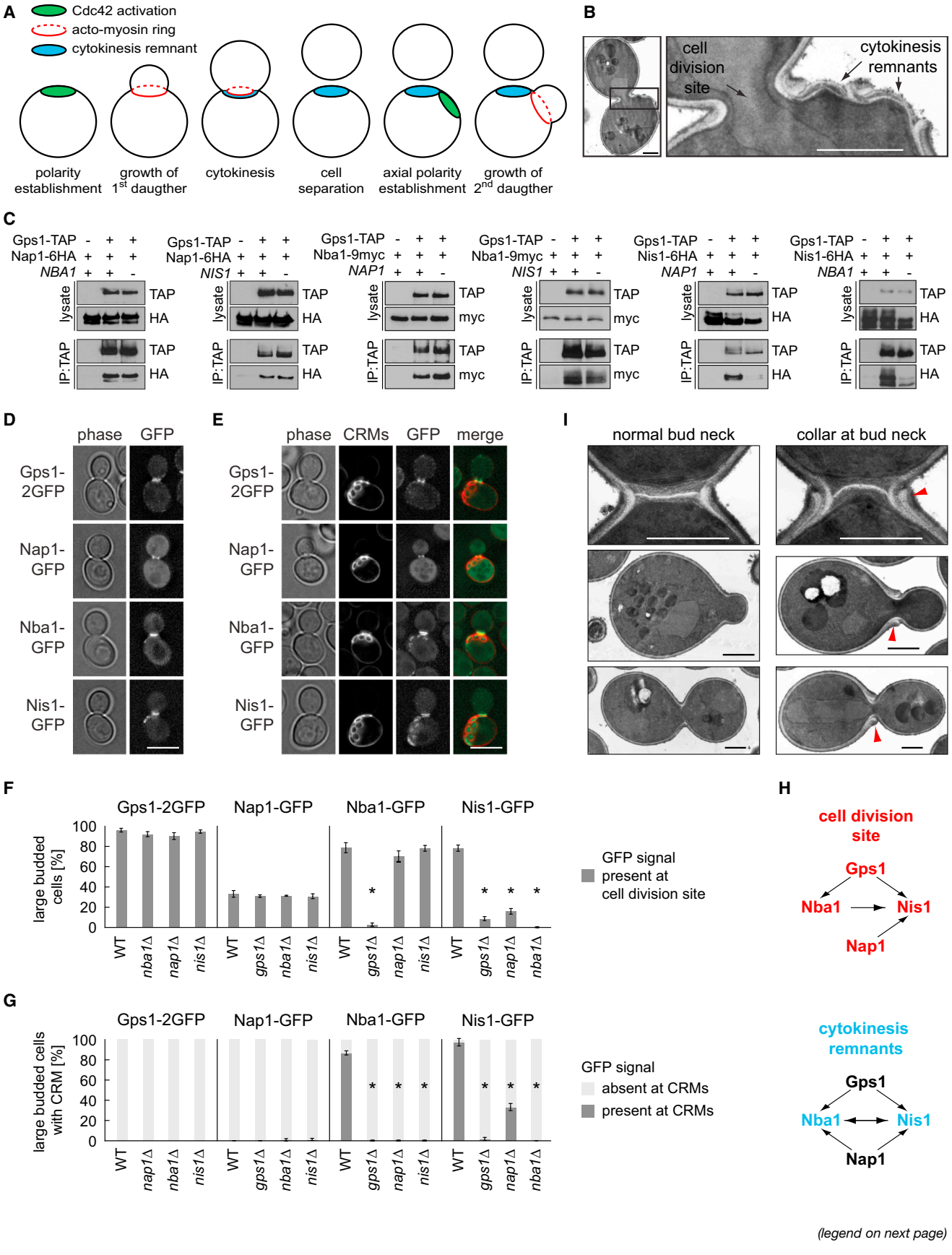

(legend on next page)

Table 1. Cdc42 Phenotype and Rho1 Phenotype of Different Mutants

No.		Genotype	Cells with Indicated Number of Collars (%)				Septum Thickness (nm) Mean (SD)	p Value	n
A			0	1	2	>2			
	1	Wild-type	100	0	0	0	274 (98)	—	108
	2	*gps1Δ*	64	28	7	1	128 (51)	<0.001	77
	3	*nba1Δ*	61	31	8	0	231 (85)	0.006	51
	4	*nis1Δ*	95	5	0	0	266 (98)	0.6	44
	5	*nap1Δ*	97	3	0	0	361 (107)	<0.001	38
	6	*rax1Δ*	96	4	0	0	258 (108)	0.4	46
	7	*rax2Δ*	94	6	0	0	297 (107)	0.2	48
	8	*rga1Δ*	44	40	14	2	317 (113)	0.01	43
	9	*rga1Δ nba1Δ*	34	38	22	6	272 (95)	0.9	49
	10	*rsr1Δ*	100	0	0	0	ND	ND	33
	11	*nba1Δ rsr1Δ*	100	0	0	0	ND	ND	37
	12	*rga1Δ rsr1Δ*	81	19	0	0	ND	ND	63
	13	*nba1Δ rga1Δ rsr1Δ*	72	22	4	2	ND	ND	54
B	1	*gps1Δ GPS1*	100	0	0	0	318 (140)	—	27
	2	*gps1Δ*	65	30	5	0	118 (44)	<0.001	37
	3	*gps1Δ gps1-Δ301-422*	98	3	0	0	274 (98)	0.2	64
	4	*gps1Δ gps1-Δ443-530*	100	0	0	0	332 (116)	0.6	38
	5	*gps1Δ gps1-Δ513-598*	62	31	7	0	322 (113)	0.8	42
C	1	*NBA1-GFP*	100	0	0	0	231 (76)	—	49
	2	*NBA1-GFP gps1Δ*	60	32	4	4	94 (44)	<0.001	50
	3	*NBA1-GFP gps1Δ SHS1-GBP*	98	2	0	0	98 (39)	<0.001	44
D	1	*NIS1-GFP*	100	0	0	0	205 (73)	—	31
	2	*NIS1-GFP gps1Δ*	62	29	6	3	71 (19)	<0.001	34
	3	*NIS1-GFP gps1Δ SHS1-GBP*	98	2	0	0	89 (39)	<0.001	42

ND, not determined.

activation of Cdc42, the formation of a trimeric complex composed of the Cdc42 guanine nucleotide exchange factor (GEF) Cdc24, the scaffold protein Bem1 and the p21-activated (PAK) kinase Cla4, which can be reconstituted in vitro using recombinant proteins (Figures S3A and S3B) (Bose et al., 2001; Kozubowski et al., 2008), and the recruitment of Cdc24 by the Ras-related GTPase Rsr1 (Park et al., 1997; Shimada et al., 2004; Smith et al., 2013). We sought to determine whether Nba1 affects activation of Cdc42 by these two mechanisms.

In yeast two-hybrid experiments, Nba1 interacted with Bem1 and Cdc24 (Figure 3A). In vitro binding experiments suggested that these interactions are direct, because recombinant Nba1 associated with recombinant Cdc24 and Bem1 in vitro (Figure 3B). Moreover, Nba1 colocalized with Cdc24 and Bem1 at the cell-division site and with Bem1 at the emerging CRMs (Figures 3C–3F). In contrast, Nis1 did not associate with Cdc24 or Bem1 in the yeast two-hybrid system (Figure 3A) or in vitro (Figure S3C), suggesting that Nis1 does not play a direct role in regulating Cdc24. In vitro competition assays revealed that Cdc24

Figure 1. Nba1, Nis1, and Nap1 Function with Gps1 in the Cdc42 Pathway

(A) The illustration depicts active Cdc42 (green), which leads to the growth of the daughter cell. The actomyosin ring (red) forms at the same site where Cdc42 initially established polarity. After cytokinesis, this site is marked by cytokinesis remnants (blue, bud scars).

(B) Electron micrograph of a dividing yeast cell. The enlarged box shows the cell-division site and two cytokinesis remnants. Scale bars, 1.0 μm.

(C) Immunoprecipitation using cell lysates of the indicated genotypes. TAP, tandem and affinity purification tag.

(D and E) Localization of Gps1, Nap1, Nba1, and Nis1 at the cell-division site (D) and at cytokinesis remnants (CRMs) (E). CRMs were stained with calcofluor. Scale bar, 5 μm.

(F) Quantification of (D). Only large-budded cells were counted, n > 100 cells per strain. *p < 0.0001.

(G) Quantification of (E). Only cells with CRMs were counted, n > 100 cells per strain. *p < 0.0001. See Figure S1C for additional p values of (F) and (G). Data in (F) and (G) are represented as mean ± SEM of three independent experiments.

(H) Diagrams summarizing the dependence in protein localization at the bud neck or CRMs as scored in (F) and (G).

(I) Electron micrographs showing cross-sections of the bud-neck region (cell-division site) of wild-type (normal bud neck) and *nba1Δ* (collar at bud neck) cells. The arrowhead points toward a bud-neck collar, which is indicative of Cdc42 activation at the same site of cytokinesis, thereby causing budding inside the old cell-division site. Scale bar, 1 μm. See also Figure S1.

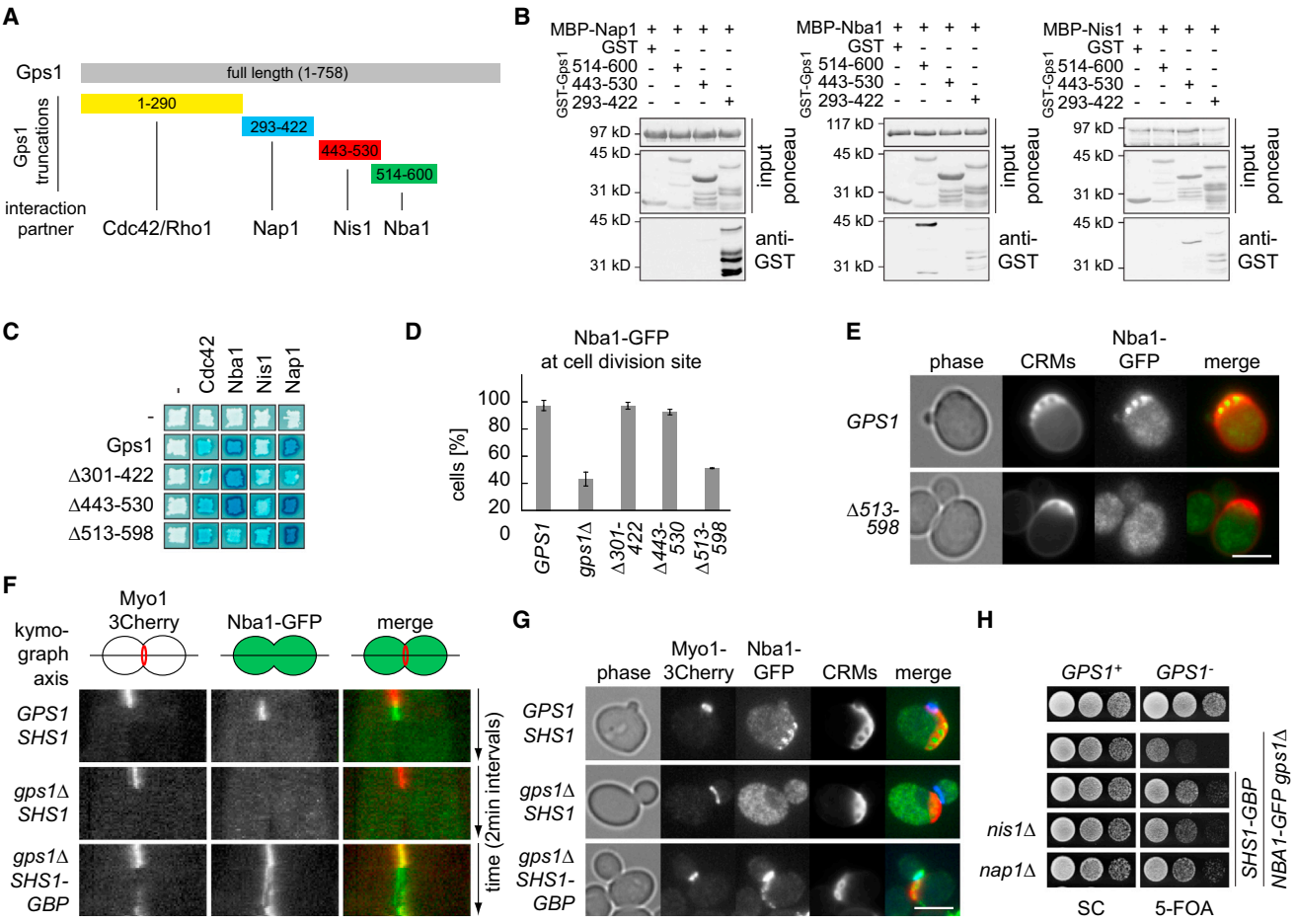

Figure 2. Nba1 Is Required and Sufficient to Inhibit Cdc42 Activation

(A) Schematic representation of the Gps1 fragments that specifically interact with Rho1/Cdc42, Nap1, Nis1, and Nba1 (see also Figure S2A). Numbers indicate amino acid positions.

(B) In vitro binding assays showing the binding of GST or the indicated GST-Gps1 fragments to beads coupled to MBP-Nap1, MBP-Nba1, or MBP-Nis1. Ponceau-S-stained nitrocellulose membranes show the inputs for MBP (top panels) and GST (middle panels) fusion proteins.

(C) Yeast two-hybrid analysis of Gps1 full-length and truncated forms lacking the indicated amino acids. Blue color denotes interaction.

(D) Quantification of Nba1 localization at the cell-division site in the indicated Gps1 truncated mutants. Only large-budded cells were counted (n > 100 per strain). Data are represented as mean ± SEM of three independent experiments.

(E) Localization of Nba1 at CRMs. In all inspected cells (n > 100 per strain), Nba1 localized at CRMs in *GPS1* but not in *gps1-Δ513-598* cells. CRMs were stained with calcofluor.

(F) Artificial tethering of Nba1-GFP in wild-type and *gps1Δ* cells at the cell-division site using the GFP binding protein (GBP) fused to the septin Shs1. Kymographs of the daughter-mother axis are shown. Each pixel represents one time point. Myo1-3Cherry, which disappears from the cell-division site after cytokinesis, was used as a cell-cycle marker.

(G) Localization of Nba1-GFP at CRMs in *GPS1*, *gps1Δ SHS1*, and *gps1Δ SHS1-GBP* cells carrying Myo1-3Cherry. CRMs were stained with calcofluor.

(H) Growth test showing serial dilutions of the strains with the indicated genotypes and carrying an *URA3*-based plasmid expressing wild-type *GPS1*. Cells were spotted on SC-complete plates (maintain *URA3-GPS1*) and on 5FOA plates (selects against *URA3-GPS1*). Scale bars, 5 μm. See also Figure S2.

bound to Nba1 only when Bem1 was either absent or present in substochiometric amounts (Figure 3G, lanes 3–6). Similarly, Bem1 associated with Nba1 only in the presence of low levels of Cdc24 (Figure 3G, lanes 9–12). However, Nba1 was not able to disassemble or to prevent the assembly of Cdc24-Bem1-Cla4 complexes in vitro (Figures S3D and S3E). Therefore, we reasoned that Nba1 binds to Cdc24 and Bem1 to prevent a different activation step.

We next tested whether Nba1 affects the binding of Cdc24 to Rsr1. As previously reported, Cdc24 preferentially bound recombinant Rsr1 that was locked in the GTP-bound state (Figure 3H, lanes 1 and 3) (Park et al., 1997). Strikingly, Cdc24 did not associate with GTP-bound Rsr1 in the presence of Nba1 (Figure 3H, lane 2), suggesting that Nba1 could inhibit the activation of Cdc24 by Rsr1. We tested this possibility in vivo using two mutants of Cdc24: $Cdc24^{\Delta PB}$, which cannot bind to Bem1 (Kozubowski et al., 2008), and $Cdc24^{G168D}$, which is unable to bind Rsr1 (Shimada et al., 2004). Deletion of *NBA1* rescued the growth defect of a *cdc24Δ* strain expressing the $cdc24^{\Delta PB}$ mutant but not the $cdc24^{G168D}$ mutant (Figures 3I and S3F),

suggesting that activation of Cdc24$^{\Delta PB}$ by Rsr1 is not sufficient to support growth due to negative regulation by Nba1. In conclusion, our data support a model in which Nba1 locally prevents activation of the guanine nucleotide exchange factor Cdc24 by Rsr1, thereby inhibiting Cdc42 activity at the cell-division site and CRMs (Figure 3J).

The Transmembrane Proteins Rax1 and Rax2 Anchor Nba1 and Nis1 at CRMs

Puzzlingly, Nba1 and Nis1 directly interact with Gps1 and require Gps1 for their localization to both the cell-division site and CRMs, but Gps1 is only associated with the cell-division site. Nba1 and Nis1 have no obvious transmembrane or membrane-binding domains, suggesting they likely rely on a protein other than Gps1 as an anchor at CRMs. Rax1 and Rax2, two transmembrane proteins of unknown function in haploid cells, stably localize to CRMs in an interdependent manner (Chen et al., 2000) (Figures S4A and S4B). We found that *RAX1* and *RAX2* were required for the localization of Nba1 and Nis1 to CRMs but not to the cell-division site, without affecting the total protein levels of Nba1 and Nis1 (Figure 4). Deletion of *RAX1* or *RAX2* impaired Cdc42 inhibition to the same extent as deletion of *NIS1*, as judged by the percentage of cells with multiple collar phenotype (Table 1A). Yeast two-hybrid analysis revealed that Nis1 interacted with the C-terminal cytoplasmic tail of Rax2 in a *NAP1*-dependent manner (Figures S4C–S4E). Deletion of the 37 C-terminal residues of Rax2 (Rax2-ΔC) impaired Nis1 and Nba1 localization to CRMs (Figures S4F and S4G). However, Rax1 also failed to localize to CRMs in *rax2-ΔC* cells (Figure S4H), suggesting that the C-terminal tail of Rax2 is critical for Rax1-Rax2 complex formation. The recruitment of Gps1 or Nap1 to the cell-division site was not influenced by *RAX1* or *RAX2* deletions (data not shown). Together, these results place Rax1 and Rax2 in the Cdc42 inhibition pathway and indicate that Rax1 and Rax2 serve as a binding platform for Nba1 and Nis1 at CRMs.

Nba1 and Nis1 Are Transferred from the Cell-Division Site to the Emerging CRM

We next investigated the mechanism by which Nba1 and Nis1 localize to CRMs. We considered two possibilities: Nba1 and Nis1 could be loaded onto CRMs from a cytoplasmic pool ("diffusion model") or Nba1 and Nis1 could be transferred, directly or indirectly, from the site of cell division to Rax1-Rax2 at CRMs ("inheritance model"). Two observations suggest that Nba1 and Nis1 must associate with Gps1 and Nap1 at the cell-division site before it becomes a CRM with cell separation, and thus favor the inheritance model. First, Gps1 and Nap1 are restricted to the cell-division site, yet both proteins are required for Nis1 and Nba1 localization to CRMs (Figures 1D–1H). Second, artificial tethering of Nba1 and Nis1 to the cell-division site partially restored Nba1 and Nis1 association with CRMs in *gps1Δ* cells (Figure 2G and S2C). To directly examine Nba1 and Nis1 loading to CRMs, we performed a pulse-chase experiment using cells expressing *NIS1-GFP* under control of the galactose-inducible promoter (*pGal1*) (Figure 5A). Without promoter induction, no Nis1-GFP could be detected in *pGal1-NIS1-GFP* cells (Figure 5A, t = −2 hr). After a 2 hr pulse of induction, Nis1-GFP was detected initially only at the cell-division site and later at the newly emerging (proximal) but not at the older (distal from the bud neck) CRMs (Figure 5A, t = 0 and 2 hr). Similar results were obtained for Nis1-GFP in pulse-chase experiments with inducible expression of *NBA1* or *RAX1* (Figure S5A). Moreover, Nba1-GFP behaved in an analogous manner in similar experiments (Figures 5A and S5A). These results indicate that Nba1 and Nis1 must associate with the cell-division site before it is converted into a CRM.

Interestingly, Nis1-GFP and Nba1-GFP were found exclusively at distal CRMs 8 hr after the expression pulse (Figure 5A), suggesting that both proteins associate with CRMs in a stable manner. Supporting this notion, analysis of protein age with a tandem fluorescent protein timer (tFT) composed of the fast-maturing green fluorescent protein sfGFP and the slower-maturing red fluorescent protein mCherry (Khmelinskii et al., 2012) showed that Nba1 and Nis1 pools are on average older at CRMs than at the cell-division site (Figure 5B), similar to Rax2, which is known to be stably associated with CRMs (Chen et al., 2000; Khmelinskii et al., 2012). Moreover, in fluorescence recovery after photobleaching experiments, Nis1-GFP showed no detectable turnover at CRMs over a period of more than 4 hr, whereas Nba1-GFP underwent slow turnover at CRMs (half-time >30 min) (Figures 5C, 5D, and S5B; data not shown).

Collectively, our results are consistent with a model in which Nis1 and Nba1 need to associate with the cell-division site to become stably recruited to CRMs, where Nis1 recruits Nba1 through a series of successive steps that required Gps1, Nap1, and Rax1-Rax2 (Figures 1H, 4, and 5E).

Cell-Division Site Reuse Impairs Nuclear Segregation and Shortens Replicative Lifespan

Deletion of the gene coding for Rga1, a GTPase-activating protein (GAP) for Cdc42, was previously reported to result in rebudding at the most recent site of cell division (Tong et al., 2007). We therefore tested whether Rga1 and Nba1 cooperate in preventing the reuse of previous cell-division sites. Transmission electron microscopy showed that the percentage of cells with multiple collars at the bud neck was higher in the *rga1Δ nba1Δ* double mutant than in either single mutant (Table 1A). We conclude that Rga1 and Nba1 cooperate in inhibiting rebudding at CRMs. However, whereas Rga1 prevents Cdc42 reactivation at the most recent CRM, Nba1 also prevents Cdc42 reactivation at older CRMs with the help of Gps1, Nap1, Nis1, Rax1, and Rax2.

Next, we sought to determine the physiological significance of preventing rebudding from CRMs. We followed single cells through consecutive divisions until cell death using a microfluidics-based long-term live cell imaging technique (Fehrmann et al., 2013) with a GFP-tagged histone H2B (Htb2) to visualize nuclear segregation (Figure 6A). Whereas wild-type cells divided on average 20 times before death (replicative lifespan) in this assay, the replicative lifespan of cells lacking *NBA1* and *RGA1* alone or in combination was significantly shorter (Figures 6A and 6B). The short replicative lifespan of *nba1Δ* and *rga1Δ* cells was clearly distinct from the frequent premature cell death observed in *gps1Δ* cells (Meitinger et al., 2013). The thinning of the secondary septum observed specifically in *gps1Δ* cells (Table 1A) leads to the lysis of daughter cells during cytokinesis

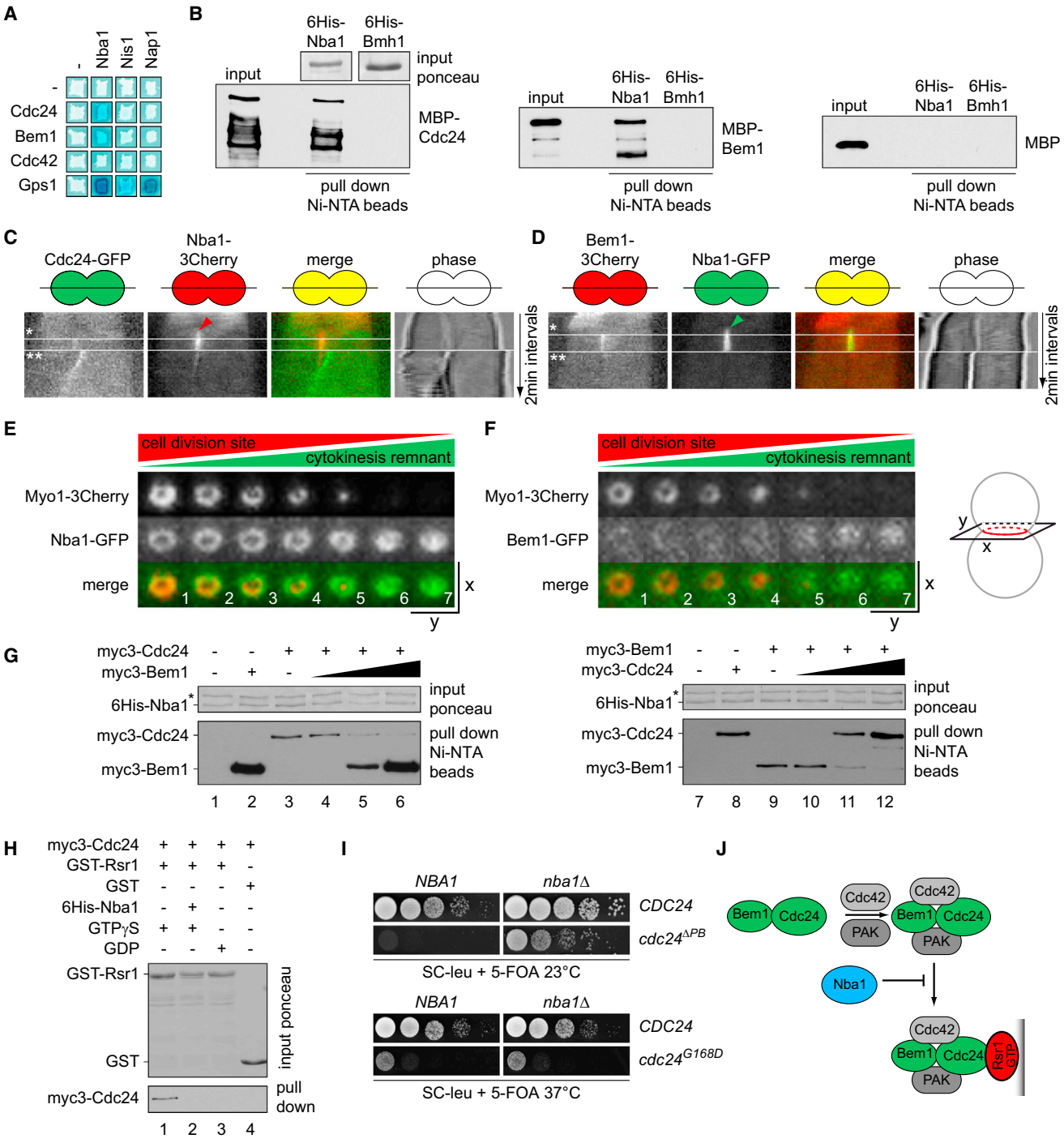

Figure 3. Nba1 Directly Interacts with Cdc24 and Bem1 and Inhibits the Binding of Cdc24 to GTP-Bound Rsr1

(A) Yeast two-hybrid interaction of Nba1, Nis1, and Nap1 with Cdc24, Bem1, Cdc42, and Gps1. The blue color indicates interaction.

(B) In vitro binding assay using recombinant proteins. Immobilized 6His-Nba1 was incubated with MBP alone, MBP-Cdc24, or MBP-Bem1 as indicated. The 14-3-3 family protein Bmh1 was used as a negative control.

(C and D) Kymographs of the daughter-mother cell axis show the colocalization of Cdc24 and Nba1 (C) or Bem1 and Nba1 (D) at the cell-division site. Each pixel represents one time point. Nba1 appears at the cell-division site before Cdc24 (7.1 ± 2.0 min, n = 15) or Bem1 (8.1 ± 1.7 min, n = 17). Arrowhead, appearance of Nba1 at the cell-division site; *, appearance of Cdc24 and Bem1 at the cell-division site; **, cell separation.

(E and F) Time-lapse series showing top view of Nba1-GFP (E) or Bem1-GFP (F) at the cell-division site during actomyosin ring contraction (Myo1-3Cherry).

(legend continued on next page)

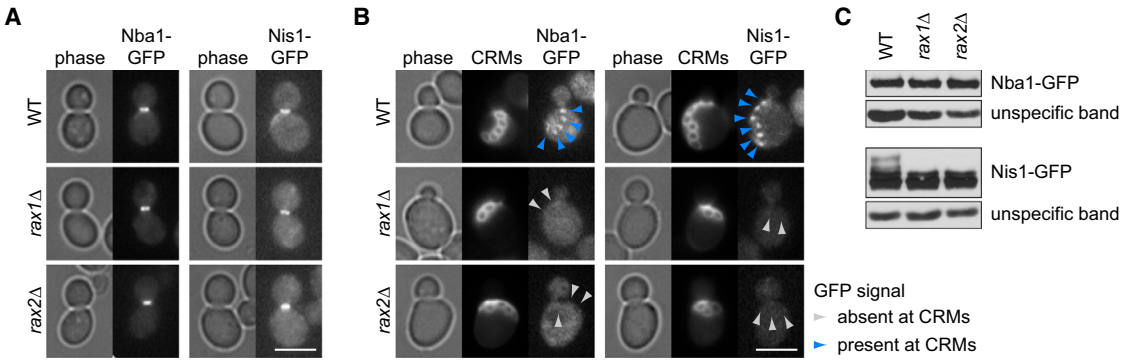

Figure 4. The Transmembrane Proteins Rax1 and Rax2 Target Nba1 and Nis1 to Cytokinesis Remnants

(A and B) Localization of Nba1-GFP and Nis1-GFP at the cell-division site (A) or CRMs (B) in wild-type, *rax1Δ*, and *rax2Δ* cells (n > 100 for each strain). Arrows point to CRMs. CRMs were stained with calcofluor. Scale bar, 5 μm.

(C) Immunoblots showing the protein amounts of Nba1-GFP and Nis1-GFP in wild-type, *rax1Δ*, and *rax2Δ* cells using anti-GFP antibodies. An unspecific band served as a loading control. See also Figure S4.

(Meitinger et al., 2013). As a result, an asynchronous *gps1*Δ (but not *nba1*Δ, *rga1*Δ, or *nba1*Δ *rga1*Δ) population contained ~30% of dead cells and exhibited reduced doubling time (Figures S6A and S6B).

We thus examined the premature cell death phenotype of the *nba1*Δ *rga1*Δ mutant in more detail. We determined the time that it took to segregate the nucleus into the daughter cell body in each cell division and complete anaphase throughout the course of replicative aging. Wild-type cells completed nuclear segregation in less than 20 min, with some sporadic delays (Figure 6C). Nuclear segregation delays became more frequent in wild-type cells after entry into senescence, which was scored as a sudden increase in the duration of cell cycle (Fehrmann et al., 2013) (Figures 6C and 6D). In contrast, delayed nuclear segregation was frequent even in young (i.e., nonsenescent) *nba1Δ rga1Δ* cells and often immediately preceded cell death (Figures 6A, 6C, and 6D), suggesting that these cells died prematurely as a consequence of a defective mitosis. Consistently, nuclear segregation into the daughter compartment frequently failed in *nba1Δ rga1Δ* cells, resulting in binucleated cells (Figures 6C and 6D).

How could reuse of previous cell-division sites cause defects in nuclear segregation? We observed that the diameter of the bud-neck opening was narrower in cells with multiple collars, which underwent rebudding from CRMs (Figures 6E and 6F). Moreover, the replicative lifespan of the *nba1*Δ, *rga1*Δ, and *nba1*Δ *rga1*Δ cells negatively correlated with the frequency of rebudding from CRMs, as judged by the percentage of cells with bud-neck collars (Figure 6G). We reasoned that narrowing of the bud neck due to repeated rebudding from the same site could hinder nuclear segregation into the daughter cell, thus explaining the nuclear segregation defects and shortened lifespan of *nba1*Δ *rga1*Δ cells. Supporting this hypothesis, deletion of *RSR1*, which results in Cdc24 mislocalization and random budding (Chant and Herskowitz, 1991), reduced the percentage of *nba1Δ rga1Δ* cells with bud-neck collars (Table 1A) and significantly rescued the survival rate of *nba1Δ rga1Δ* cells (Figure 6H).

Collectively, our data strongly suggest that the relocation of the site of bud growth makes a significant contribution to the fidelity of nuclear segregation and is required to ensure a robust replicative lifespan.

DISCUSSION

Although it is long recognized that Cdc42 activation is never established twice at the same site in yeast, the underlying molecular mechanisms and physiological significance of such a regulation remain elusive. Here, we show that CRMs of budding yeast are marked by Cdc42 inhibitory complexes. We identified the protein Nba1 as a core subunit of these complexes and show that Nba1 directly regulates Cdc42. In vitro analyses combined with in vivo functional studies establish that Nba1 spatially inhibits the activation of Cdc42 by impeding the interaction between the Cdc24 GEF, Cdc24, and its upstream activator, the GTPase Rsr1. This study therefore reveals Nba1 as a player that

(G) In vitro competition assay using bacterial purified proteins. Left panel: immobilized Nba1 was incubated with buffer only (lane 1), myc3-Bem1 (lane 2), and myc3-Cdc24 in the absence (lane 3) or presence of increasing amounts of Bem1 (lanes 4–6). Right panel: same as before but using a constant amount of myc3-Bem1 and variable amounts of myc3-Cdc24. Asterisk, unspecific protein.

(H) Nba1 interrupts the interaction of GTP-Rsr1 with Cdc24. Immobilized GST-Rsr1 was incubated with GTPγS (lanes 1 and 2), GDP (lane 3), or buffer only (lane 4). GST-Rsr1 beads were incubated with myc3-Cdc24 protein extract in the absence (lane 1) or presence (lane 2) of 6His-Nba1. GST only was used as a negative control (lane 4). Myc3-Cdc24 was detected using anti-myc antibodies.

(I) Growth of *cdc24Δ NBA1 URA3-CDC24* or *cdc24Δ nba1Δ URA3-CDC24* cells carrying a *LEU2*-based plasmid containing full-length *CDC24*, $cdc24^{\Delta PB}$ (*CDC24* codons 1–750), or $CDC24^{G168D}$ (glycine 168 substituted to glutamic acid) as indicated. Serial dilution of cells were spotted on SC-LEU (*URA3-CDC24* is retained) and 5FOA-LEU2 (*URA3-CDC24* is lost) plates and incubated at 23°C or 37°C for 3 days (see Figure S4E for growth at different temperatures).

(J) Summary of Nba1 interactions. Our data indicate that Nba1 binds directly to Bem1 and Cdc24 and inhibits Cdc24 binding to Rsr1 at CRMs. See also Figure S3.

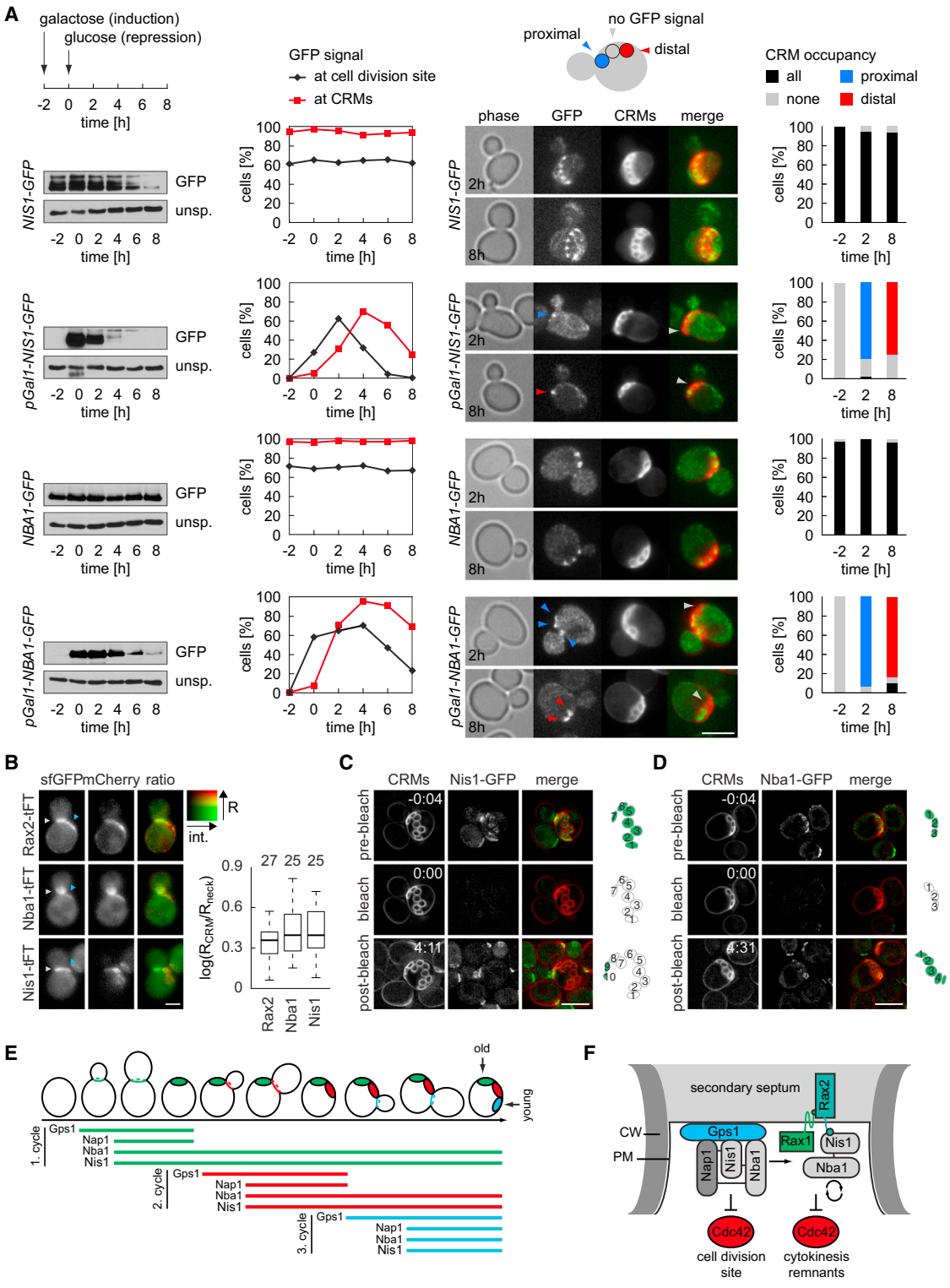

Figure 5. Nba1 Is Inherited at Cytokinesis Remnants by a Two-Step Mechanism

(A) Pulse-chase experiments using *NIS1-GFP*, pGal1-*NIS1-GFP*, *NBA1-GFP*, or pGal1-*NBA1-GFP* cells were performed as illustrated in the time diagram. The expression of genes under control of the galactose promoter was induced for a period of 2 hr, allowing the accumulation of the corresponding protein. After repression of the galactose promoter (addition of glucose, t = 0), the localization of the indicated GFP-tagged proteins was analyzed over time. CRMs were stained with calcofluor. Newly formed CRMs located proximal to the new emerging daughter cell (blue), whereas older ones locate more distally (red). Protein

(legend continued on next page)

constrains Rsr1 function and acts alongside landmark proteins, which are involved in the spatial control of bud site selection (Casamayor and Snyder, 2002). Our data further establish that the inhibitory mode of Nba1 action upon Cdc42 differs from the control of GTP hydrolysis that is orchestrated by the GAP protein Rga1. Accordingly, epistasis studies established that Rga1 and Nba1 collaborate in the inhibition of Cdc42, because cells lacking both proteins reused the same polarity site for Cdc42 activation with a higher frequency than cells lacking either regulator alone. However, in contrast to Rga1, which is confined to the site of cell division, Nba1 remains associated with older CRMs. Our data thus indicate that Nba1 functions as a molecular spatial memory that confers protection from recurrent Cdc42 polarization at the same site. We propose that CRMs are marked with "negative polarity cues" that prevent Cdc42 reactivation.

We previously reported that Gps1 binds Cdc42 and prevents Cla4-mediated polarity establishment at the cell-division site (Meitinger et al., 2013). However, it was not clear how this inhibition was achieved on a molecular level. We found that Gps1 directly interacts with Nba1 and Cdc42. Because Gps1 is dispensable for the inhibition of Cdc42-Cla4-mediated polarity establishment upon artificial targeting of Nba1 to the cell-division site (Figure 2), the inhibition of Cla4 by Gps1 is most likely a consequence of the upstream inhibition of Cdc42 that occurs at the level of Cdc24. We thus favor the idea that Gps1 acts as a scaffold protein at the cell-division site that supports local inactivation of Cdc42 by Nba1.

We describe an elaborated system of three successive steps (recruitment, transfer/inheritance, and maintenance) that are absolutely required to load Nba1 onto CRMs. First, Gps1 recruits Nba1 and the adaptor protein Nis1 to the cell-division site. At this site, the chaperone Nap1 is essential for the transfer of Nba1 and Nis1 from Gps1 to the transmembrane proteins Rax1-Rax2. Nba1 then remains associated with Rax2 at CRMs in a Nis1-dependent manner. Based on localization and deletion analysis, we propose the existence of two complexes that associate with CRMs of different ages. The Gps1/Nba1/Nis1/Nap1 complex is present only at emerging CRMs (cell-division site), whereas the Rax1/Rax2/Nis1/Nba1 complex associates with older CRMs and maintains this association over multiple generations. Importantly, disruption of Nba1 at emergent CRMs causes a more severe Cdc42 inhibition phenotype than Nba1 removal from established older remnants (e.g., in *nis1Δ*, *nap1Δ*, *rax1Δ*, or *rax2Δ* cells). We therefore reasoned that inhibition of Cdc42 at the most recent site of cell division is more critical than its inhibition at older CRMs. This might explain why cells also rely on the GAP Rga1 to prevent Cdc42 activation at the cell-division site (Tong et al., 2007).

Why have cells developed such an elaborated mechanism to maintain and protect CRMs? In the absence of Nba1 and/or Rga1, the replicative lifespan of yeast cells was significantly shorter than in wild-type controls. This shortening of lifespan correlated with nuclear segregation defects that, in most cases, immediately preceded cell death. We previously reported that cells lacking *GPS1* had an increased rate of cell death that was exacerbated by codepletion of *RGA1* (Meitinger et al., 2013). However, several evidences support that cell death of *nba1Δ rga1Δ* and *gps1Δ* cells are caused by different mechanisms. First, *nba1Δ rga1Δ* cells do not show a defect in cell growth as *gps1Δ* cells do (Figure S6). Second, in contrast to *gps1Δ* mutants, whose daughter cells selectively dye during cytokinesis (Meitinger et al., 2013), we mainly observed cell death of large-budded *nba1Δ rga1Δ* cells shortly after binucleation (Figure 6). Third, the growth defect of *gps1Δ* cells is based on the misregulation of the Rho1-pathway (Meitinger et al., 2013), which is functional in *nba1Δ rga1Δ* cells (Table 1). We thus propose that the narrowing of the bud-neck diameter by repeated reuse of the same polarity site was the most likely cause of nuclear segregation defects and cell death in *nba1Δ rga1Δ* cells. In support of this assumption, we found that deletion of *RSR1*, which decreased the probability of reuse of the cell-division site for bud growth, improved the survival rate of *nba1Δ rga1Δ* cells. We thus propose that the combined impact of the different Cdc42 cell polarity control mechanisms guarantees genome stability and the fitness of dividing cells. In light of our study, many open questions remain. For example, it is unclear why yeast cells developed such a complex system for protecting CRMs against Cdc42 repolarization when other cell types simply remove CRMs (Pohl and Jentsch, 2009). It also begs the question as to whether CRMs may play other mother cell-specific functions that are yet to be appreciated, perhaps during the aging process itself.

levels were analyzed using anti-GFP antibodies. An unspecific band served as a loading control. The graphs represent the quantification of the percentage of large-budded cells showing Nba1-GFP at the cell-division site or CRMs (only cells with CRMs were counted). Images show representative cells analyzed at early (2 hr) or late (8 hr) time points after repression of the galactose promoter. The graphs on the right indicate the percentage of cells with the given GFP-tagged protein at none, all, only proximal, or only distal CRMs ("CRM occupancy"). Only cells with more than one CRM were counted. n > 100 cells per time point. CRMs were stained with calcofluor.

(B) Nba1, Nis1, and Rax2 are fused to the tandem fluorophore sfGFP-mCherry. The ratio between mCherry and sfGFP fluorescence intensities at the cytokinesis remnants (R_{CRM}) and the cell-division site (R_{neck}) are used to determine the age of the different protein pools. The graph shows the logarithm of the ratio of R_{CRM} and R_{neck}. $\log(R_{CRM}/R_{neck}) > 0$ indicates that the protein pool at cytokinesis remnants is older than at the cell-division site.

(C and D) Fluorescence recovery of Nis1-GFP (C) and Nba1-GFP (D) at CRMs 4.5 hr after photobleaching. The numbers on the right indicate CRMs pre- and postbleach; the green color indicates the presence of the GFP fusion protein at the given CRM. CRMs were stained with calcofluor.

(E) Model for the timely loading of Nba1 and Nis1 to CRMs based on pulse-chase (A), age determination (B), FRAP experiments (C and D), and localization studies (Figure 1). The aforementioned data indicate that Gps1 is recruited to the newly formed bud neck and recruits Nba1 and Nis1 to the cell-division site of large-budded cells. After cell separation, Nis1 and Nba1 but not Gps1 or Nap1 remain stably associated with the emerging CRM as the new bud emerges. Each color represents one generation in which the proteins are attached to CRMs.

(F) Model for the formation of a Gps1 dependent complex at the cell-division site. During cytokinesis, Nba1 and Nis1 are transferred to the transmembrane protein Rax2, which depends on the chaperone Nap1. Both complexes are necessary to prevent Cdc42 activation at the cell-division site and at CRMs. CW, cell wall; PM, plasma membrane and secondary septum are indicated. Scale bars, 5 μm. See also Figure S5.

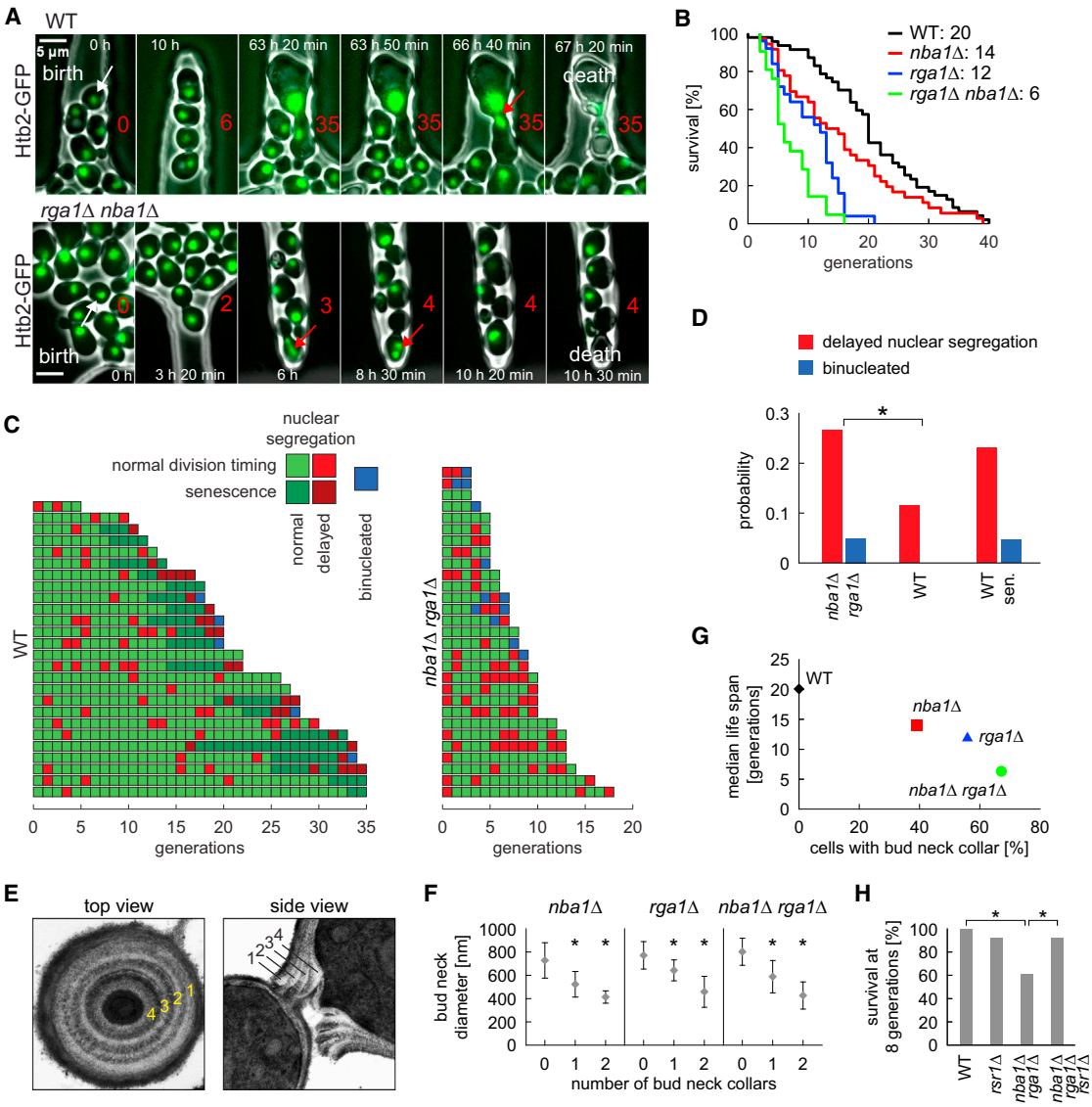

Figure 6. Inhibition of Cdc42 at Cytokinesis Remnants Contributes to the Fidelity of Nuclear Segregation and Longevity

(A) Time-lapse series of wild-type (WT) and *nba1Δ rga1Δ* single cells from birth to death in the microfluidic device at the indicated time points. The histone, Htb2 tagged with GFP, was used as a nuclear marker. The white arrows indicate the cells that became trapped in the cavity. Red numbers indicate how many buds the cell generated since birth. Red arrows mark nuclear segregation delays and binucleated cells.

(B) Survival probability curves of wild-type (WT, n = 47), *nba1Δ* (n = 36), *rga1Δ* (n = 25), and *nba1Δ rga1Δ* (n = 21) cells. The median survival is indicated. All mutants display a significantly reduced longevity compared to WT ($p < 0.001$).

(C) Temporal trajectories showing successive divisions of single cells. Green, red, and blue colors indicate normal anaphase (<20 min), delayed anaphase (>20 min), and binucleated cells, respectively. Dark colors indicate when cells have entered senescence.

(D) Quantification of the probability per generation of delayed nuclear segregation (>20 min, red bars) or binucleation (blue bars) to occur. The difference between *nba1Δ rga1Δ* and young wild-type cells was significant ($p < 0.001$). Senescent wild-type cells were scored separately.

(E) TEM transverse (top view) and longitudinal (side view) sections of *nba1Δ* cells with four collars at the bud-neck region, as indicative of recurrent rebudding at the same location.

(F) Quantification of the bud-neck diameter of *nba1Δ*, *rga1Δ*, and *nba1Δ rga1Δ* cells with different numbers of bud-neck collars (no collar, n = 20; one collar, n = 18; twos collar, n = 18). Data are represented as mean ± SEM. *$p < 0.001$.

(G) Graph depicting the percentage of cells with multiple collars (determined in F) versus the median lifespan (determined in B) for the indicated strains.

(H) Percentage of surviving cells at eight generations for the indicated cell types was calculated based on single-cell analysis performed as described in (A) (n = 40 for each strain). Note that, due to the random budding pattern of *rsr1Δ* cells, the time that the mother cell remained in the inspection chamber was limited to seven to nine generations. *$p < 0.001$. See also Figure S6.

Molecular remnants of the cell-division site persist at the plasma membrane of daughter cells in several organisms and do so in a cell-type-specific manner. For example, stem cells mimic budding yeast, in accumulating division remnants in successive cell divisions (Chen et al., 2013). Thus, it is tempting to speculate that also in other organims the cytokinetic machinery may act as platform that allows the specific and asymmetric inheritance of associated protein complexes, which might affect cell fate determination. CRMs have recently been implicated in determining the spatial orientation and establishment of cell polarity in neurons (Pollarolo et al., 2011; Wilcock et al., 2007). Interestingly, Cyk4 (a metazoan inhibitor of the Rho GTPase Rac1) persists at cell-division remnants of *C. elegans* (Bastos et al., 2012; Jantsch-Plunger et al., 2000), and this persistence has been implicated in positioning the centrosome and cell-division plane during early embryonic cell divisions (Hyman, 1989; Keating and White, 1998; Waddle et al., 1994). Thus, it is tempting to speculate that CRMs play a conserved role in affecting cell polarity by acting as a spatial memory in a variety of organisms ranging from yeast to higher eukaryotes.

EXPERIMENTAL PROCEDURES

Yeast Methods and Plasmid Construction

Yeast strains and plasmids used in this study are listed in Tables S1 and S2. For bacterial expression, genes or gene fragments were cloned into pGEX-5X-1 (GST, GE Healthcare), pET28c (6His, Novagen), and pMAL-c2x (MBP, NEB). Yeast growth and media were as described (Sherman, 1991). Gene deletions and epitope tagging were performed using PCR-based methods (Janke et al., 2004; Knop et al., 1999). Genes of interest were expressed from their endogenous promoter unless specified otherwise. Yeast strains were grown in yeast peptone dextrose medium containing 0.1 mg/l adenine (YPAD). Strains carrying plasmids were grown in synthetic complete (SC) media lacking the corresponding amino acids. Loss of *URA3*-containing plasmids was assessed by using plates containing 1 mg/ml 5-fluoroorotic acid (5FOA).

Genetic Interactions Based on Growth

The plasmid shuffle strategy was used to test the viability of single and double mutants (genetic interaction). Briefly, mutant strains containing the corresponding wild-type gene on an *URA3*-based plasmid (pRS316) were analyzed for growth on 5FOA plates (selection against *URA3*). At least six individual transformants were analyzed for each mutant, and one representative mutant is shown. For each mutant 10-fold serial dilutions of wild-type (ESM356-1) and mutants with the indicated genotype were spotted onto SC and 5FOA plates. Mutants were complemented by pRS316-*GPS1* (Figures 2H and S2D) or pRS316-*CDC24* (Figures 3I and S3G). Strains carrying genes on a *LEU2*-based plasmid (Figures 2H, 3I, and S3G) were grown on medium lacking leucine to avoid plasmid loss. Plates were incubated for 1 or 2 days at 30°C.

Protein Detection Methods and Quantifications

Yeast protein extracts and Immunoblotting were performed as described (Janke et al., 2004). Antibodies were rabbit anti-GFP antibody, mouse anti-tubulin (Tub1), mouse anti-HA (clone 12CA5, Sigma), mouse anti-Myc (clone 9E10, Sigma), rabbit anti-Clb2, rabbit anti-TAP (Open Biosystems), mouse anti-MBP (NEB), and guinea pig anti-GST. Secondary antibodies were goat anti-mouse, goat anti-rabbit, and goat anti-guinea pig immunoglobulin Gs coupled to horseradish peroxidase (Jackson ImmunoResearch Laboratories). Protein concentrations were determined using Bradford reagent accordingly to manufactures' instructions (Bio-Rad). Immunoprecipitation, in vitro binding, and yeast two-hybrid assays are described in Extended Experimental Procedures.

Microscopy Techniques

For fluorescence still image analysis, cells carrying GFP or Cherry fusion proteins were inspected without fixation (Figures 1D, 1E, 2A–2D, 3C–3F, 5B–5D, S1B, S2B, S4A, S4B, S4F–S4H, S5B, and S6A) or after fixation with 4% formaldehyde for 20 min (Figures 2E, 2G, 4A, 4B, 5A, S2C, and S5A). CRMs were stained with 0.1 mg/ml calcofluor (Fluorescence Brightener 28, Sigma-Aldrich). Live-cell imaging and quantification of fluorescence still images were performed as described in Extended Experimental Procedures. The tandem fluorescent protein timer experiment for Rax2, Nba1, and Nis1 was performed and quantified as described in Extended Experimental Procedures (Khmelinskii et al., 2012). Long-term FRAP analysis for Nba1 and Nis1 was performed in observation chambers of a Y4C microfluidic plate (CellAsic) at 30°C as described in Extended Experimental Procedures (Khmelinskii et al., 2012). Specimens for electron microscopy were prepared as described previously in Extended Experimental Procedures (Meitinger et al., 2011).

Replicative Lifespan Analysis in a Microfluidic Device

Time-lapse images (phase contrast and fluorescence) were acquired using a microfluidic device as described previously (Fehrmann et al., 2013) using an automated epifluorescence microscope (Nikon Eclipse Ti) with a digital CMOS camera (Hamamatsu Orca Flash 4.0). Cells were grown in synthetic complete medium and then were loaded into the device and allowed to divide until death during typically 100 hr. Constant media perfusion allowed keeping the cells in exponential growth during the course of the experiment. Replicative lifespans were analyzed from time-lapse images (one frame every 10 min). Survival curves were calculated from the number of buds produced by individual mother cells. Nucleus segregation defects were scored using a nuclear marker (Htb2-GFP).

SUPPLEMENTAL INFORMATION

Supplemental Information includes Extended Experimental Procedures, six figures, and two tables and can be found with this article online at http://dx.doi.org/10.1016/j.cell.2014.10.014.

ACKNOWLEDGMENTS

We thank Daniel Lew for reagents; Karsten Richter and DKFZ electron microscopy facility for support with electron microscopy; Daniela T. Bertazzi Lazzarini for working with Nba1 and Nis1 at the initial phase of this project; Elmar Schiebel, Iain Hagan, and members of G.P.'s lab for comments on the manuscript. G.C. was supported by the Atip Avenir program and the IDEX program from the University of Strasbourg. S.M. acknowledges a fellowship from the French Ligue Nationale contre le Cancer. M.K. and A.K. were supported by the Sonderforschungsbereich 1036 (SFB1036, TP10) from the DFG. The work of F.M., S.P., and A.A.-P. was supported by the Marie Curie Grant MEXT-CT-042544 granted to G.P. S.P. acknowledges funding from the graduate school LGFG ''Regulation of Cell Division''. S.P. and B.K. are members of the international graduate school HBIGS. This project was funded by the Marie Curie Grant MEXT-CT-042544 and DKFZ core funding.

Received: March 10, 2014
Revised: August 20, 2014
Accepted: September 25, 2014
Published: November 13, 2014

REFERENCES

Atkins, B.D., Yoshida, S., Saito, K., Wu, C.F., Lew, D.J., and Pellman, D. (2013). Inhibition of Cdc42 during mitotic exit is required for cytokinesis. J. Cell Biol. *202*, 231–240.

Bastos, R.N., Penate, X., Bates, M., Hammond, D., and Barr, F.A. (2012). CYK4 inhibits Rac1-dependent PAK1 and ARHGEF7 effector pathways during cytokinesis. J. Cell Biol. *198*, 865–880.

Bloch, D., and Yalovsky, S. (2013). Cell polarity signaling. Curr. Opin. Plant Biol. *16*, 734–742.

Bose, I., Irazoqui, J.E., Moskow, J.J., Bardes, E.S., Zyla, T.R., and Lew, D.J. (2001). Assembly of scaffold-mediated complexes containing Cdc42p, the exchange factor Cdc24p, and the effector Cla4p required for cell cycle-regulated phosphorylation of Cdc24p. J. Biol. Chem. *276*, 7176–7186.

Boureux, A., Vignal, E., Faure, S., and Fort, P. (2007). Evolution of the Rho family of ras-like GTPases in eukaryotes. Mol. Biol. Evol. *24*, 203–216.

Cabib, E., Mol, P.C., Shaw, J.A., and Choi, W.J. (1993). Biosynthesis of cell wall and septum during yeast growth. Arch. Med. Res. *24*, 301–303.

Calvert, M.E., Keck, K.M., Ptak, C., Shabanowitz, J., Hunt, D.F., and Pemberton, L.F. (2008). Phosphorylation by casein kinase 2 regulates Nap1 localization and function. Mol. Cell. Biol. *28*, 1313–1325.

Casamayor, A., and Snyder, M. (2002). Bud-site selection and cell polarity in budding yeast. Curr. Opin. Microbiol. *5*, 179–186.

Chant, J., and Herskowitz, I. (1991). Genetic control of bud site selection in yeast by a set of gene products that constitute a morphogenetic pathway. Cell *65*, 1203–1212.

Chen, T., Hiroko, T., Chaudhuri, A., Inose, F., Lord, M., Tanaka, S., Chant, J., and Fujita, A. (2000). Multigenerational cortical inheritance of the Rax2 protein in orienting polarity and division in yeast. Science *290*, 1975–1978.

Chen, C.T., Ettinger, A.W., Huttner, W.B., and Doxsey, S.J. (2013). Resurrecting remnants: the lives of post-mitotic midbodies. Trends Cell Biol. *23*, 118–128.

Dworkin, J. (2009). Cellular polarity in prokaryotic organisms. Cold Spring Harb. Perspect. Biol. *1*, a003368.

Etienne-Manneville, S. (2004). Cdc42—the centre of polarity. J. Cell Sci. *117*, 1291–1300.

Fehrmann, S., Paoletti, C., Goulev, Y., Ungureanu, A., Aguilaniu, H., and Charvin, G. (2013). Aging yeast cells undergo a sharp entry into senescence unrelated to the loss of mitochondrial membrane potential. Cell Reports *5*, 1589–1599.

Heasman, S.J., and Ridley, A.J. (2008). Mammalian Rho GTPases: new insights into their functions from in vivo studies. Nat. Rev. Mol. Cell Biol. *9*, 690–701.

Howell, A.S., and Lew, D.J. (2012). Morphogenesis and the cell cycle. Genetics *190*, 51–77.

Hyman, A.A. (1989). Centrosome movement in the early divisions of Caenorhabditis elegans: a cortical site determining centrosome position. J. Cell Biol. *109*, 1185–1193.

Iden, S., and Collard, J.G. (2008). Crosstalk between small GTPases and polarity proteins in cell polarization. Nat. Rev. Mol. Cell Biol. *9*, 846–859.

Ishimi, Y., and Kikuchi, A. (1991). Identification and molecular cloning of yeast homolog of nucleosome assembly protein I which facilitates nucleosome assembly in vitro. J. Biol. Chem. *266*, 7025–7029.

Iwase, M., and Toh-e, A. (2001). Nis1 encoded by YNL078W: a new neck protein of Saccharomyces cerevisiae. Genes Genet. Syst. *76*, 335–343.

Janke, C., Magiera, M.M., Rathfelder, N., Taxis, C., Reber, S., Maekawa, H., Moreno-Borchart, A., Doenges, G., Schwob, E., Schiebel, E., and Knop, M. (2004). A versatile toolbox for PCR-based tagging of yeast genes: new fluorescent proteins, more markers and promoter substitution cassettes. Yeast *21*, 947–962.

Jantsch-Plunger, V., Gönczy, P., Romano, A., Schnabel, H., Hamill, D., Schnabel, R., Hyman, A.A., and Glotzer, M. (2000). CYK-4: A Rho family gtpase activating protein (GAP) required for central spindle formation and cytokinesis. J. Cell Biol. *149*, 1391–1404.

Johnson, D.I., and Pringle, J.R. (1990). Molecular characterization of CDC42, a Saccharomyces cerevisiae gene involved in the development of cell polarity. J. Cell Biol. *111*, 143–152.

Johnson, J.M., Jin, M., and Lew, D.J. (2011). Symmetry breaking and the establishment of cell polarity in budding yeast. Curr. Opin. Genet. Dev. *21*, 740–746.

Kang, P.J., Angerman, E., Nakashima, K., Pringle, J.R., and Park, H.O. (2004). Interactions among Rax1p, Rax2p, Bud8p, and Bud9p in marking cortical sites for bipolar bud-site selection in yeast. Mol. Biol. Cell *15*, 5145–5157.

Keating, H.H., and White, J.G. (1998). Centrosome dynamics in early embryos of Caenorhabditis elegans. J. Cell Sci. *111*, 3027–3033.

Khmelinskii, A., Keller, P.J., Bartosik, A., Meurer, M., Barry, J.D., Mardin, B.R., Kaufmann, A., Trautmann, S., Wachsmuth, M., Pereira, G., et al. (2012). Tandem fluorescent protein timers for in vivo analysis of protein dynamics. Nat. Biotechnol. *30*, 708–714.

Knop, M., Siegers, K., Pereira, G., Zachariae, W., Winsor, B., Nasmyth, K., and Schiebel, E. (1999). Epitope tagging of yeast genes using a PCR-based strategy: more tags and improved practical routines. Yeast *15* (10B), 963–972.

Kozubowski, L., Saito, K., Johnson, J.M., Howell, A.S., Zyla, T.R., and Lew, D.J. (2008). Symmetry-breaking polarization driven by a Cdc42p GEF-PAK complex. Curr. Biol. *18*, 1719–1726.

Li, R., and Bowerman, B. (2010). Symmetry breaking in biology. Cold Spring Harb. Perspect. Biol. *2*, a003475.

Martin-Belmonte, F., and Perez-Moreno, M. (2011). Epithelial cell polarity, stem cells and cancer. Nat. Rev. Cancer *12*, 23–38.

McCaffrey, L.M., and Macara, I.G. (2009). Widely conserved signaling pathways in the establishment of cell polarity. Cold Spring Harb. Perspect. Biol. *1*, a001370.

Meitinger, F., Boehm, M.E., Hofmann, A., Hub, B., Zentgraf, H., Lehmann, W.D., and Pereira, G. (2011). Phosphorylation-dependent regulation of the F-BAR protein Hof1 during cytokinesis. Genes Dev. *25*, 875–888.

Meitinger, F., Richter, H., Heisel, S., Hub, B., Seufert, W., and Pereira, G. (2013). A safeguard mechanism regulates Rho GTPases to coordinate cytokinesis with the establishment of cell polarity. PLoS Biol. *11*, e1001495.

Mortensen, E.M., McDonald, H., Yates, J., 3rd, and Kellogg, D.R. (2002). Cell cycle-dependent assembly of a Gin4-septin complex. Mol. Biol. Cell *13*, 2091–2105.

Nelson, W.J. (2009). Remodeling epithelial cell organization: transitions between front-rear and apical-basal polarity. Cold Spring Harb. Perspect. Biol. *1*, a000513.

Noatynska, A., Tavernier, N., Gotta, M., and Pintard, L. (2013). Coordinating cell polarity and cell cycle progression: what can we learn from flies and worms? Open Biol *3*, 130083.

Park, H.O., and Bi, E. (2007). Central roles of small GTPases in the development of cell polarity in yeast and beyond. Microbiol. Mol. Biol. Rev. *71*, 48–96.

Park, H.O., Bi, E., Pringle, J.R., and Herskowitz, I. (1997). Two active states of the Ras-related Bud1/Rsr1 protein bind to different effectors to determine yeast cell polarity. Proc. Natl. Acad. Sci. USA *94*, 4463–4468.

Pohl, C., and Jentsch, S. (2009). Midbody ring disposal by autophagy is a post-abscission event of cytokinesis. Nat. Cell Biol. *11*, 65–70.

Pollarolo, G., Schulz, J.G., Munck, S., and Dotti, C.G. (2011). Cytokinesis remnants define first neuronal asymmetry in vivo. Nat. Neurosci. *14*, 1525–1533.

Rothbauer, U., Zolghadr, K., Muyldermans, S., Schepers, A., Cardoso, M.C., and Leonhardt, H. (2008). A versatile nanotrap for biochemical and functional studies with fluorescent fusion proteins. Mol. Cell. Proteomics *7*, 282–289.

Sherman, F. (1991). Getting started with yeast. Methods Enzymol. *194*, 3–21.

Shimada, Y., Wiget, P., Gulli, M.P., Bi, E., and Peter, M. (2004). The nucleotide exchange factor Cdc24p may be regulated by auto-inhibition. EMBO J. *23*, 1051–1062.

Smith, S.E., Rubinstein, B., Mendes Pinto, I., Slaughter, B.D., Unruh, J.R., and Li, R. (2013). Independence of symmetry breaking on Bem1-mediated autocatalytic activation of Cdc42. J. Cell Biol. *202*, 1091–1106.

Tong, Z., Gao, X.D., Howell, A.S., Bose, I., Lew, D.J., and Bi, E. (2007). Adjacent positioning of cellular structures enabled by a Cdc42 GTPase-activating protein-mediated zone of inhibition. J. Cell Biol. *179*, 1375–1384.

Waddle, J.A., Cooper, J.A., and Waterston, R.H. (1994). Transient localized accumulation of actin in Caenorhabditis elegans blastomeres with oriented asymmetric divisions. Development *120*, 2317–2328.

Wilcock, A.C., Swedlow, J.R., and Storey, K.G. (2007). Mitotic spindle orientation distinguishes stem cell and terminal modes of neuron production in the early spinal cord. Development *134*, 1943–1954.

Wloka, C., and Bi, E. (2012). Mechanisms of cytokinesis in budding yeast. Cytoskeleton *69*, 710–726.